Environmental and biological controls on Mg and Li in deep-sea scleractinian corals

David H. Case,[a,*] Laura F. Robinson,[a] Maureen E. Auro,[a] Alexander C. Gagnon[b]

[a]Department of Marine Chemistry and Geochemistry
Woods Hole Oceanographic Institution
360 Woods Hole Road, Mail Stop 25
Woods Hole, MA 02543
USA

[b]Earth Sciences Division and The Molecular Foundry
Lawrence Berkeley National Laboratory
1 Cyclotron Road, Mail Stop 67R3208
Berkeley, CA 94720
USA

[*]Corresponding author
Tel: 608-443-8880

Email addresses:
dcase@caltech.edu (D.H. Case)
lrobinson@whoi.edu (L.F. Robinson)
mauro@whoi.edu (M.E. Auro)
acgagnon@lbl.gov (A.C. Gagnon)

Abstract

Deep-sea scleractinian corals precipitate aragonite skeletons that provide valuable archives of past ocean conditions. During calcification biological mediation causes variability in trace metal incorporation and isotopic ratios of the aragonite such that signals caused by environmental controls can be overwhelmed. This complicates the interpretation of geochemical proxies used for paleo-reconstructions. In this study we examine the environmental controls on the Mg/Li ratio of 34 individuals from seven genera of deep-sea scleractinian corals: *Desmophyllum*, *Balanophyllia, Caryophyllia, Enallopsammia*, *Flabellum, Trochocyanthus*, and *Lophelia.* In addition we examine the distributions of Mg and Li in *Desmophyllum* and *Balanophyllia* using laser ablation inductively coupled plasma mass spectrometry (LA-ICP-MS).

Both Mg/Ca and Li/Ca ratios increased by more than a factor of 2 in the center of calcification regions compared to the outer, fibrous regions of the coral skeleton. As a result, replicate ~10 mg subsamples of coral show less variability in the Mg/Li ratio than Mg/Ca. Microscale Mg and Li results are consistent with Rayleigh-type incorporation of trace metals with additional processes dominating composition within centers of calcification. Comparison of Mg/Li to seawater properties near the site of collection shows that the ratio is not controlled by either carbonate ion or salinity. It appears that temperature is the major control on the Mg/Li ratio. For all 34 samples the temperature correlation (R^2=0.62) is significantly better than for Mg/Ca (R^2=0.06). For corals of the family *Caryophyllidae* the R^2 value increases to 0.82 with the exclusion of one sample that was observed to have an altered, chalky texture. Despite this excellent correlation the scatter in the data suggests that the Mg/Li ratio of deep-sea corals

cannot be used to reconstruct temperature to better than approximately ±1.6°C without better temperature control and additional calibration points on modern coral samples.

Keywords: biomineralization, paleoceanography, deep-sea coral, Mg/Ca, Mg/Li, thermometry

1. Introduction

Ice core records show that there have been large and abrupt changes in atmospheric temperature in the past, as particularly well documented during the last deglaciation (Grootes et al., 1993). Since approximately half of the cross-equatorial heat transport occurs in the ocean (Ganachaud and Wunsch, 2000) there are likely to be important links between ocean circulation and climate (Rahmstorf, 2002). High-resolution, well-dated records of deep-water temperatures are difficult to obtain because of the challenges of bioturbation and constructing precise chronologies in sediment cores. Using the skeletons of deep-sea corals to reconstruct seawater temperature in the past would circumvent some of these challenges given a suitable geochemical proxy for temperature.

Deep-sea corals inhabit a wide variety of depths and geographic distributions, including high-latitude regions and all ocean basins (Cairns, 2007). Scleractinian corals are made of aragonite and datable using U/Th techniques, allowing accurate and precise ages to be calculated for each individual (Cheng et al., 2000). Solitary deep-sea scleractinians have been collected from diverse settings, and fossil specimens in existing collections span hundreds of thousands of years (e.g., Robinson et al., 2006). *Desmophyllum dianthus*, a species that has been used in a

number of paleo-studies, live on the order of 100 years providing potential centennial-scale archives (Adkins et al., 1998).

Despite the promise of deep-sea corals for reconstructing past ocean circulation, paleoceanographic reconstruction of temperature has been complicated by vital effects. This broad term represents the influence of biomineralization on skeletal composition. The near constant environmental conditions of the deep sea over the roughly 100 year lifetime of modern corals and the lack of photosymbionts mean that compositional variability in the coral skeleton can be attributed entirely to the processes of coral biomineralization.

Stable isotopes and trace element ratios commonly used in paleoceanography, including $\delta^{13}C$, $\delta^{18}O$, Mg/Ca, Sr/Ca, and U/Ca all vary across deep-sea scleractinian skeletal features (Adkins et al., 2003; Cohen et al., 2006; Gagnon et al., 2007; Robinson et al., 2006; Sinclair et al., 2006; Smith et al., 2000; Smith et al., 2002). The magnitude of this variation changes from proxy to proxy, but for temperature reconstructions can overwhelm environmental controls. Much of the compositional variability in coral follows differences in skeletal architecture. On the macroscale, corals contain septal and thecal features, the former being comprised of septa radiating about the axis of the coral and the latter comprising the thick walls of the coral structure. Scleractinian coral skeletons have two distinctive micro-scale architectures: the Centers of Calcification (COCs) which contain small, granular, disorganized crystals, and the surrounding region which are comprised of fibrous bundles of aragonite needles (Gladfelter, 1982; Stolarski, 2003; Gladfelter, 2007). These features have also been documented in scleractinian deep-sea corals (Adkins et al., 2003; Robinson et al., 2006; Gagnon et al., 2007; Rollion-Bard et al., 2010). In the deep-sea coral *D. dianthus*, Mg/Ca nearly doubles in the COCs (Gagnon et al., 2007), while $\delta^{13}C$ and $\delta^{18}O$ are depleted (Adkins et al., 2003). These results may

113 be interpreted as evidence that separate mechanisms control composition in different regions of
114 the coral skeleton. However, Sr/Ca seems unaffected by skeletal architecture (Gagnon et al.,
115 2007) while [U] is lower in regions associated with, but extending beyond, the COCs (Robinson
116 et al., 2006), suggesting some continuity of mechanism across the whole coral skeleton.
117 Geochemical models of biomineralization attempt to explain the mechanisms controlling
118 the distribution of trace metals and isotopes in coral skeletons. Models can be distinguished by
119 the most important step or process proposed to control skeletal composition. Some of these
120 processes include ion transport, pH-driven solution chemistry (e.g.: McConnaughey, 1989;
121 Adkins et al., 2003), precipitation from a closed system (e.g.: Gaetani & Cohen, 2006; Cohen et
122 al., 2006; Gagnon et al., 2007), the role of an organic matrix during precipitation, and the
123 presence of transient amorphous phases (Rollion-Bard et al., 2010). In this paper we examine Mg
124 and Li in *D. dianthus* accompanied by a discussion of mechanisms controlling the incorporation
125 and variation of these elements.
126 Most existing models agree that coral skeletogenesis occurs in a biologically controlled
127 space with a unique composition called the "extracytoplasmic calcifying fluid," or ECF
128 (Johnson, 1982; McConnaughey, 1989; Adkins et al., 2003). The source and transport of skeletal
129 ions into the ECF has the potential to affect skeletal composition and cause vital effects. While
130 the extent of seawater leakage and its influence on calcification is a matter of debate, transport of
131 bulky fluorescent dyes to the skeleton implicates direct seawater transport (Erez & Braun, 2007).
132 Consideration of the ECF as a closed system has prompted the application of Rayleigh
133 fractionation principles to trace metal incorporation (Gaetani & Cohen, 2006; Cohen et al., 2006;
134 Gagnon et al., 2007; Rollion-Bard et al., 2009). This class of model describes a system in which
135 trace metals are precipitated into the aragonite lattice from an ECF that initially matches the

136 seawater composition, but is subsequently closed with regard to ion transport. As precipitation
137 proceedes the ECF becomes depleted in calcium and depleted or enriched in trace metals
138 depending on their distribution coefficient. Cohen et al. (2006) and Gagnon et al. (2007) have
139 applied this theory to model Sr/Ca and Mg/Ca variability in deep-sea corals where Sr has a
140 distribution coefficient >1 while that of Mg is <<1. Gagnon et al. (2007) concluded that Rayleigh
141 fractionation is consistent with their correlated Me/Ca variability outside of obvious *D. dianthus*
142 COCs. However, an equally important conclusion of that study is that large Mg/Ca variability
143 associated with COCs is dominated by a mechanism other than a Rayleigh process
144 The pathway for incorporation of Mg in aragonite is not well constrained (Fallon et al.,
145 2003). While Mg^{2+} may be directly substituted for Ca^{2+} as has been documented in calcite (Politi
146 et al., 2010) the relatively small ionic radius of Mg^{2+} severely distorts the 6-fold coordinated
147 calcite lattice, and it is likely that the aragonite lattice of scleractinian corals would be even more
148 severely distorted. However since Mg is typically much less abundant in aragonite than in
149 calcite, the effect of such distortions may be less significant. Finch & Allison (2008) employed
150 X-ray Absorption Fine Structure (XAFS) to determine the structural state of Mg in scleractinian
151 coral samples and the authors interpret their results to indicate that Mg is not directly hosted in
152 aragonite. These data may mean Mg is located in disordered a site, consistent with either organic
153 binding or the presence of amorphous calcium carbonate (ACC). Alternatively Mg^{2+} in corals
154 may be loosely bound in the aragonite lattice or adsorbed to crystal surfaces (Amiel et al., 1973;
155 Walls et al., 1977). Regarding Li incorporation, much less is known. Li^{+} incorporation has been
156 observed in inorganic aragonite experiments (Okumura & Kitano, 1986), but Li^{+} substitution for
157 Ca^{2+} is more complicated than Mg^{2+} because of the difference in charge. We compare some of
158 these mechanisms to our data in the discussion.

Bryan & Marchitto (2008) discovered a strong Mg/Li-to-temperature correlation in the shells of calcitic and aragonitic foraminifera which was significantly better than that for Mg/Ca. This study evaluates major environmental controls on Mg/Li by comparing the measured ratio of seven genera of deep-sea corals with ambient seawater. We also build on our understanding of coral vital effects and geochemistry by analyzing the microscale distribution of Mg and Li in *D. dianthus* and *Balanophyllia*.

2. Materials and Methods

2.1 Sample selection

Thirty-four separate coral individuals representing seven scleractinian genera were selected: *Desmophyllum* (n=22), *Balanophyllia* (n=4), *Caryophyllia* (n=3), *Flabellum* (n=1), *Trochocyanthus* (n=1), *Enallopsammia* (n=2), and *Lophelia* (n=1) (Table 1). The first five are solitary corals while the latter two are colonial. The samples were selected to represent diverse oceanographic settings in all major ocean basins (Figure 1), and cover a depth range of 120 to 1818 meters. Environmental parameters, including temperature, salinity, and carbonate ion concentration were derived from the GLODAP database (Key et al., 2004, Table 1). Typically, the match between coral and water column location was within 3.5° latitude and longitude and closer than 30 meters in depth.

Corals in this study were either loaned from the Smithsonian Museum of Natural History by Stephen Cairns or collected on recent cruises to the North Atlantic or Southern Ocean. Corals from recent cruises were either collected live or were radiocarbon dated to be recently dead

182 (Burke et al., in press, available online). For the case of the Southern Ocean samples temperature
183 and salinity were also available from nearby CTD casts taken on the same cruise, *Nathaniel B.*
184 *Palmer* 0805.
185 The temperature range for all samples is from 1.8 to 17.0°C. Salinity ranged from 34.04
186 to 36.54 ‰ and carbonate ion concentration from 1.2 to 192.7 μmol/kg (Table 1). Samples from
187 the Smithsonian museum were assumed to be modern, although two (48738 and 77019)
188 exhibited a visibly chalky texture indicating that they may have experienced post-mortem
189 alteration.
190
191 *2.2 Sample preparation*
192
193 Coral samples were prepared for two different types of analyses: bulk solution ICP-MS
194 and laser ablation ICP-MS. For bulk solution ICP-MS, samples ranging from 10 to 136 mg were
195 cut from the coral using a dremel tool. Subsamples came from both thecal and septal regions, and
196 some coral individuals were subsampled more than once. At most four subsamples were taken
197 from a single coral individual. All corals were chemically cleaned at WHOI using the oxidative
198 and reductive steps of Cheng et al. (2000). After cleaning, samples were dissolved in 5% Optima
199 Grade nitric acid, diluted to 60 ppm Ca, and spiked to 0.5 ppb In.
200 To prepare for ICP-MS laser ablation, sections of coral were cut perpendicular to the
201 coral growth axis with a dremel saw, bound to a microscope slide using epoxy (polymerized
202 Araldite resin, Ernest F. Fullam, Inc.) and polished with 0.18 μm silica. Images of each section
203 were taken under reflected light.
204

205 *2.3 Standard mixing for ICP-MS*

206

207 Gravimetric elemental solutions were prepared for two standard curves to account for
208 matrix effects, background corrections and differences in elemental ionization. The first set had
209 constant Me/Ca ratios diluted into five solutions with concentrations of Ca varying from 8.8 to
210 79.6 ppm. The second standard series contained constant Sr, Ba, Mg, and Li concentrations but
211 varying Ca concentrations over a range of 0 to 175 ppm, encompassing ranges broadly observed
212 in coral skeletons (McCulloch et al., 2003; Gagnon et al., 2007; Allison et al., 2007; Mitsuguchi
213 et al., 2008). A separately mixed Fe (16 ppb), Mn (16 ppb), and Ca (57 ppm) standard was also
214 prepared. All standards and solution samples were spiked to 0.5 ppb In to monitor ICP-MS
215 intensity drift.

216

217 *2.4 Bulk solution ICP-MS*

218

219 Solution samples were run on a Thermo Element2 ICP-MS, tuned to yield at least
220 275,000 counts per second (cps) for a 0.5 ppb In solution. Full standard curves were run at the
221 beginning and end of each session and between every 10-15 samples. A consistency standard,
222 S13, and 5% Optima Grade nitric acid blanks were run between every four samples. Every coral
223 sample aliquot was measured twice. The isotopes ^{7}Li, ^{25}Mg, ^{48}Ca, ^{88}Sr, and ^{138}Ba were measured
224 in low resolution with a mass resolving power of 300 (M/ΔM at 5% peak height). Medium-
225 resolution mode was used for ^{55}Mn and ^{56}Fe. For each isotope the sampling time was 0.03
226 seconds, except for ^{7}Li which was increased to 0.30 seconds. Counting mode was used to
227 measure ^{7}Li, ^{115}In, ^{138}Ba, ^{55}Mn, and ^{56}Fe while ^{48}Ca and ^{88}Sr were measured in analog mode.

228 ^{25}Mg varied between counting and analog modes (~$4e^6$ cps). The method collected 600 cycles of
229 data per sample giving a total analysis time of ~3 minutes. Background corrections were made
230 by subtracting the intensity of bracketing acid blanks from standard and sample intensities. Rinse
231 time was three minutes between each sample resulting in background ^{7}Li counts less than 100
232 cps, only ~0.5% of our typical signal. Relative standard deviations for raw ratios were better than
233 2% for all samples and standards and were typically better than 1.5% (1-σ) for $^{25}Mg/^{7}Li$,
234 $^{25}Mg/^{48}Ca$, and $^{7}Li/^{48}Ca$. Since this study focuses on Mg, Li, and Ca, henceforth we only discuss
235 these elements. Fe and Mn results are semi-quantitative and are used only for the purposes of
236 checking for contamination.
237
238 *2.5 Data correction and reproducibility*
239
240 After the background correction, a number of additional corrections were made to the raw
241 data to account for dilution, matrix effect, element-specific ionization efficiency, and
242 instrumental drift. To account for small variations in the In spikes, the measured intensities were
243 corrected to the gravimetrically determined In concentration to the intensity expected for a 0.5
244 ppb solution. This correction allows direct comparison with standards for calculating elemental
245 concentrations. However, we only report final data as ratios and not concentrations.
246 The intensity of each isotope was normalized to the average value of In during each ICP-
247 MS run to account for drift. For the standard curves, each "Observed" ratio was compared to the
248 gravimetrically determined "Expected" ratio to ascertain the relative ionization efficiency. This
249 efficiency drifted by a maximum of ~5% on any one day. Within the Ca concentration range of
250 40 to 100 ppm the Observed/Expected ratios showed that there are no biases from matrix effects

or from the background correction. Our samples were therefore diluted to 60 ppm. A consistency standard (S13) was used to test the reproducibility and accuracy, which were always within 2% of expected values, and $^{25}Mg/^{7}Li$ was generally within 1%.

The same solution standards were used for laser ablation standardization, although a blank subtraction was not applied because the solution acid blanks are not representative of the blank levels in the laser ablation chamber. We expect the laser ablation background to be smaller than for solution analyses, for which the background corrections were ~0.5%.

2.6 Laser ablation ICP-MS

Laser ablation was carried out using a 193 nm laser coupled to the same Thermo Element2 ICP-MS with the same isotopes and ratios measured as for solution analyses. The laser spot size was 50 μm and was run at a repetition of 20 Hz. Laser power was run at 100% capacity and scan speed was set at 3 μm/sec. Ablated material was mixed with a 5% Optima grade acid stream to provide a wet plasma equivalent to standard introduction. Solution standards are not ideal since they are not matrix matched to the samples, so measured laser ablation values are therefore assumed to be relative but not absolute. Even with this potential bias, our laser ablation values are well within the range of the solution data for the same coral individuals (Figure 2, Figure 3).

Three coral cross-sections were chosen for laser ablation. These included two sections from a single *D. dianthus* individual (DMC08a and DMC08b) and one from a *Balanophyllia*. Both corals were collected from the same site in the Southern Ocean (*Nathaniel B. Palmer* 0805, TB04). Long laser lines were run perpendicular to coral density strata (i.e. across skeletal

features) and short lines were run parallel to coral density strata (i.e. within single skeletal features). Each short line was run once and the standard deviations of the ratios were calculated from the discrete analysis spots along the line. These standard deviations were generally 5% or lower for $^{25}Mg/^{48}Ca$, $^{7}Li/^{48}Ca$, and $^{25}Mg/^{7}Li$, though in two cases the *Balanophyllia* $^{25}Mg/^{7}Li$ ratio approached 10%. Standard deviations of discrete analysis points for the long lines are not representative of the analytical precision since each ablation line crosses regions with large Me/Me variability. Instead the long lines were repeated up to three times in adjacent series, providing an approximation of replicate measurements (Figure 2). The long lines proved to be reproducible, often with 5% or less disagreement between adjacent lines (Figure 2).

3. Results

3.1 Laser ablation ICP-MS

Solution standardization of laser ablation is not ideal as it is not matrix matched, so we restrict our discussion of laser data to relative changes within each coral section and qualitative comparisons to biomineralization models. However, there is reasonable agreement between the data collected by laser ablation and bulk solution (Figure 2, Figure 3).

Consistent with previous studies we observed large Mg/Ca variation associated with changes in the skeletal architecture of the coral in *D. dianthus*. An overlay of trace metal data was created by matching time-stamped data to coral features based on notes taken during the laser ablation run (Figure 4). Mg/Ca was higher by more than a factor of 2 in COC regions as opposed to outer fibrous bands. The Li/Ca ratio also increased by a more than a factor of 2 in the

297 COCs. In both cases the highest values were in the central, widest band in the coral, with local
298 maxima in less well-developed COCs. The Mg/Li ratio also shows distinct variability across the
299 *D. dianthus* skeletal sections but with a change of only a factor of 1.4. The largest maxima of
300 Mg/Li are associated with the most well developed COCs, but local maxima also appear in
301 regions not dominated by well-developed COCs (Figure 4a, b).

302 The microstructure of *Balanophyllia* is composed of COCs and fibrous material that
303 radiate outward (Figure 4c, Brahmi et al., 2010). The reflected light image of the *Balanophyllia*
304 has light and dark regions that appear to be compositionally equivalent to those in *D. dianthus*
305 (Brahmi et al., 2010). The geometry of *Balanophyllia* is more complex than for *D. dianthus* so
306 the laser ablation line was curved to stay perpendicular to the skeletal features. For this reason,
307 plots of trace metal data are not overlain on reflected light images (Figure 4c). Similar to *D.*
308 *dianthus* Mg/Ca and Li/Ca ratios vary by more than a factor of 2. Mg/Li variations in
309 *Balanophyllia* were observed throughout the skeleton and are much more frequent than those of
310 Mg/Ca or Li/Ca; it does not seem that Mg/Li variability is aligned with any specific skeletal
311 features (Figure 4c).

312 Overall LA-ICP-MS Mg/Ca ratios exhibit a strong positive relationship to Li/Ca for both
313 coral species: R^2=0.94 for *D. dianthus* and R^2=0.75 for *Balanophyllia*. Similarly there is a
314 positive correlation in multiple solution analyses from the same corals. There are two notable
315 deviations from the overall trend, one in each coral species. In *D. dianthus* section DMC08b, the
316 deviation from the regular slope is observed in the highest Mg/Ca region where Li/Ca reaches a
317 plateau. By comparing this to the reflected light image it can be seen that the location of this part
318 of the data is the central, most well-developed COC. In this area there is a distinct peak in
319 Mg/Ca, but Li/Ca does not continue to increase (Figure 4b). By contrast the *Balanophyllia*

sample exhibits a deviation in the lowest Mg/Ca region where again Mg/Ca varies and Li/Ca does not (Figure 4c).

3.2 Solution ICP-MS

In total we analyzed 34 separate corals, 7 of which were subsampled more than once. For all corals the Mg/Ca ratio ranged from 1.60 to 3.51 mmol/mol, Li/Ca from 7.05 to 14.99 μmol/mol, and Mg/Li from 0.20 to 0.35 mol/mmol (Table 1). Replicate analyses of Mg/Ca, Li/Ca and Mg/Li for the same aliquots were always within our estimated reproducibility from the internal standard S13. Analyses of separate subsamples varied by at most 11% for Mg/Li, 27% Mg/Ca, and 29% for Li/Ca, demonstrating variability within coral individuals. For example coral 48738, in which 4 subsamples were analyzed, ranged from 0.19 to 0.22 mol/mmol Mg/Li, 1.77 to 2.83 mmol/mol Mg/Ca, and 9.15 to 13.7 μmol/mol Li/Ca.

The average Mn/Ca and Fe/Ca values were 0.6 μmol/mol and 2.5 μmol/mol, respectively and the maximum values were 3.9 μmol/mol and 53.9 μmol/mol, respectively. These ratios were analyzed to determine potential contamination from ferromanganese overgrowths or detrital grains. In all cases our observed Mn/Ca values fell well below the commonly applied upper limit of 100 μmol/mol (Ferguson et al., 2008; Boyle, 1983). Likewise, the maximum Fe/Ca value of 53.9 μmol/mol is below the established upper limit of 175 μmol/mol (Ferguson et al., 2008; Lea et al., 2005; Bice et al., 2005). Both limits were developed for foraminifera, but in the absence of equivalent limits for corals we found their values to be useful benchmarks. In addition we followed the convention of Steinke et al. (2010) in testing for a correlation between Mg/Ca and either Mn/Ca or Fe/Ca. In both cases no significant correlation was observed (Mg/Ca vs. Mn/Ca,

343 R^2=0.003; Mg/Ca vs. Fe/Ca, R^2=0.01). Our samples likely have low ferromanganese
344 contamination because the specimens are modern and therefore have had little time to develop
345 ferromanganese crusts.
346
347 **4. Discussion**
348
349 *4.1 Coral calcification models*
350
351 The information from the laser ablation microscale distribution of Mg coupled to Li
352 allows us to explore modes of calcification, including continual replenishment of the ECF,
353 Rayleigh fractionation, and ACC precursors or incorporation in organic materials.
354 If the ECF is entirely open, then Mg/Ca and Li/Ca should be uniform across skeletal
355 features in the absence of other driving processes; this prediction is inconsistent with our
356 observations. If Rayleigh fractionation describes the trace metal variability, then log-log plots of
357 the Me/Ca data should be linear (Gagnon et al., 2007). Both Mg and Li are preferentially
358 excluded from aragonite (i.e.: have a distribution coefficient <<1) so a Rayleigh model would
359 predict a positive correlation between the two elements, as observed in our laser data (Figure 3).
360 The positive slopes of the Mg/Ca versus Li/Ca data from DMC08a, DMC08b, and *Balanophyllia*
361 are consistent with a Rayleigh fractionation model following that of Gagnon et al. (2007) (Figure
362 3). The uncertainty within the DMC08 laser data cloud and the relative insensitivity of the model
363 to D_{Li} allows for greater than 10-fold variability of D_{Li} within the context of the model slope.
364 However most of the data are consistent with Rayleigh fractionation starting from seawater with
365 Li, Mg, and Ca concentrations of 25.9 μmol/kg (Stoffynegli & MacKenzie, 1984), 52.7 mmol/kg

366 (Broecker & Peng, 1982), and 10.27 mmol/kg (Broecker & Peng, 1982), respectively. These
367 concentrations give rise to D_{Li} and D_{Mg} equal to $2.7x10^{-3}$ and $2.9x10^{-4}$, respectively. If regions of
368 the coral are not controlled by Rayleigh fractionation then they should plot away from this
369 relationship. In *D. dianthus* there appears to be a break in slope at the highest Mg/Ca for each
370 coral (within COCs) that indicates that Rayleigh fractionation is not the only process controlling
371 coral Mg and Li distributions. This is consistent with previous studies of Sr/Ca and Mg/Ca in *D.*
372 *dianthus* that suggest a process other than Rayleigh fractionation dominates Mg/Ca behavior in
373 the COCs (Gagnon et al., 2007). Thus, our data are consistent with Rayleigh fractionation
374 occurring across the entire skeleton, with additional mechanisms for trace metal incorporation
375 occurring within COCs.
376 Rollion-Bard et al. (2009) conclude that Rayleigh-type fractionation is insufficient to
377 explain observed Li/Ca variability coupled with near constant δ^7Li values across the skeletons of
378 deep-sea corals. Since aragonite precipitation strongly discriminates against Li incorporation, the
379 Li concentration of the ECF is largely unaffected during Rayleigh fractionation. Therefore, δ^7Li
380 should remain constant (within analytical uncertainty) during Rayleigh fractionation while Li/Ca
381 varies according to the calcium concentration of the calcifying fluid. The results measured by
382 Rollion-Bard et al. (2009) are therefore not inconsistent with Rayleigh fractionation.
383 Rollion-Bard et al. (2010) suggested that ACC formation could account for observed
384 variation in trace metal ratios. ACC has been suggested as a precursor during biogenic
385 calcification (Addadi et al., 2003; Meibom et al., 2004). While evidence for ACC in coral
386 biomineralization remains inconclusive, this precursor phase does provide a possible mechanism
387 for high Mg since Mg is enriched in ACC (Addadi et al., 2003; Wang et al., 2009). If ACC is
388 indeed present during coral skeletogensis, then ACC formation in COC regions could account for

389 the high Mg within COCs observed in this study. Alternatively, scleractinian coral skeletons are
390 known to contain a small amount of organic matrix (Cuif et al., 2003; Puverel et al., 2005).
391 Given the suggestion that organic matter may host Mg in coral skeletons (Finch & Allison,
392 2008), a second possibility is that COCs are rich in Mg-hosting organics. Consistent with this
393 explanation, Brahmi et al. (2010) find organic matter to be elevated in *Balanophyllia* COCs. Our
394 observed overall similarity in Mg/Ca and Li/Ca distributions suggest that whatever mechanism is
395 controlling Mg also controls Li, perhaps unsurprising given the similar ionic radius of the two
396 elements. These incorporation and variation pathways remain speculative, but nevertheless
397 provide possible mechanisms to elevate Mg and Li within COCs.
398 Data on Mg and Li incorporation in *D. dianthus* are complemented by several previous
399 studies, which document $\delta^{13}C$, $\delta^{18}O$, [U], and Sr/Ca variability across skeletal features (Adkins et
400 al., 2003; Robinson et al., 2006; Gagnon et al., 2007). Collectively, these patterns should
401 constrain vital effect mechanisms. Unfortunately the compositional effect of ACC, organic
402 matrix components, and several other competing mechanisms on multiple proxies remains
403 unquantified. It is our hope that future laboratory-based experiments will yield testable
404 predictions to compare different mechanisms to skeletal variability across COCs.
405
406 *4.2 Environmental controls on trace metal incorporation into deep-sea corals*
407
408 *4.2.1 Strategies for reducing the biases from vital effects*
409
410 Our new data corroborate previous studies which have reported significant trace metal
411 variation across skeletal features (Adkins et al., 2003; Sinclair et al., 2006; Cohen & Gaetani,

412 2006; Gagnon et al., 2007; Rollion-Bard et al., 2009; Brahmi et al., 2010). This distinct internal
413 variability of trace metals and isotopes means that separate subsamples of the same *D. dianthus*
414 have markedly different values (e.g. Smith et al., 2000; Figure 5). For example, if we use Mg/Ca-
415 to-temperature relationships for surface scleractinian corals (Mitsuguchi et al., 1996) and the
416 range of Mg/Ca values obtained by LA-ICP-MS on DMC08, we calculate corresponding
417 temperatures of 13˚C and 2˚C. Such a large range in apparent temperature obviously precludes
418 Mg/Ca as a paleothermometer and is in line with previous literature expressing concerns
419 regarding the Mg/Ca temperature proxy (Quinn & Sampson, 2002; Fallon et al., 2003;
420 Mitsuguchi et al., 2008; Finch & Allison, 2008, Gagnon et al., 2007). We find a negative Li/Ca-
421 to-temperature relationship, consistent with a previous study (Marriott et al., 2004a). However, it
422 exhibits extensive scatter (Figure 6i).
423 Analyzing specific features of the coral skeleton could avoid the complications presented
424 by vital effects. For example, sampling purely COC or alternatively fibrous material may allow
425 for repeatable measurements and development of a useful environmental proxy. Unfortunately,
426 we have found that such microsampling is difficult, if not impossible, on typical samples by the
427 methods described in this study. Laser ablation techniques can come close to analyzing single
428 architectural units, but with the 50 μm spot size used in our study we rarely sampled only COC
429 material even within the widest band (Figure 4). Previous work using NanoSIMS with spot size
430 0.4 μm has revealed Mg concentrations up to 10 times higher in COCs than fibrous regions
431 (Meibom et al., 2004). Targeting the fibrous bands may be somewhat easier because they tend to
432 be wider, however secondary COCs are common and sometimes difficult to identify. In
433 particular, our *Balanophyllia* samples showed broad gradients between the optical bands.

Additionally, the necessity of achieving a small spot diameter to analyze discrete parts of the coral decreases the precision of the analytical measurement.

An alternative sampling strategy for overcoming the vital effect is to take many small subsamples. Smith et al. (2000) used this approach to determine the relationship between $\delta^{13}C$ and $\delta^{18}O$ in *D. dianthus*, allowing them to determine the equilibrium values related to precipitation from seawater. Adkins et al. (2003) used a similar strategy but subsampled a thin section using a micromill, and were able to subsample finely enough to detect a break in the slope between $\delta^{13}C$ and $\delta^{18}O$ within COCs. Gagnon et al. (2007) followed this strategy for trace metals and were able to discern a similarly placed break in slope of Mg/Ca to Sr/Ca. However, deciding whether any one subsample is purely COC or not requires the assignment of arbitrary cut off values. In addition, this method is labor intensive and likely not to yield the most extreme values within the skeleton. In our study, four randomly sampled 15-20 mg fragments of coral DMC08 measured by solution ICP-MS yielded Mg/Ca values from 2.05 to 2.34 mmol/mol that do not come close to capturing the full range of Mg/Ca variability detected by 50 µm spot sizes using LA-ICP-MS.

Another approach is to find geochemical proxies less affected by biomineralization. Our in situ LA-ICP-MS data show that Mg and Li behave similarly within the coral skeleton, with high values in the COC regions and low values in fibrous areas. Since deep-sea scleractinian corals appear to incorporate Mg and Li similarly, for reasons discussed above, the ratio of these two elements has the potential to be less variable within the skeleton of a single coral. Laser ablation results show less dramatic Mg/Li variation across the coral skeleton than for either Mg/Ca or Li/Ca. For example DMC08a shows three distinct Mg/Ca peaks with the largest in the central band which is 2.1 times greater than the local Mg/Ca minimum in the adjoining fibrous

layer. The Mg/Li ratio also shows three peaks, with the central one being the largest excursion, however the magnitude is reduced to a factor of 1.4, and the two other peaks are reduced to an even greater extent. In the second section, DMC08b, the broad Mg/Ca maximum from 500 to 1100 μm is not as well developed in Mg/Li and the entire section is characterized by ~10% Mg/Li variability on a <100 μm scale. This switch from few, discrete Mg/Ca peaks to higher frequency Mg/Li variability is particularly pronounced in the *Balanophyllia* section (Figure 4c).

Mg/Li is less variable across each coral section, and that variability is more evenly distributed throughout the skeleton. Therefore a randomly cut subsample is more likely to contain a representative proportion of high and low Mg/Li and be closer the average coral value than for Mg/Ca. For example, four separate subsamples comprising septal and thecal material of the coral 48738 (*D. dianthus*) gave standard deviations for Mg/Ca, Li/Ca and Mg/Li of 22%, 18% and 5% respectively. As expected in cases where multiple subsamples were taken, the Mg/Li ratios were more reproducible than were Mg/Ca (Figure 5). Since the Mg/Li variability is distributed within the skeleton, ~10 mg samples are able to give a reasonable approximation of the average value for that coral. To achieve the best possible estimate of the true ratio in each whole coral we average all data points for separate subsamples. For corals with large skeletal features, larger samples or multiple replicates should be made to provide the most representative Mg/Li estimate.

4.3 Environmental controls on Mg/Li ratios

Having established that measured Mg/Li ratios are reasonably representative of the coral skeleton, we now examine the external controls on the average coral Mg/Li. Our results from 34

480 coral individuals show a Mg/Li range of 0.20 to 0.35 mol/mmol. First we consider contamination
481 by ferromanganese crust overgrowths and detrital grains using Mn/Ca and Fe/Ca. Both ratios
482 were low, indicating that all corals were cleaned thoroughly and allowing us to rule out
483 contamination. Second, we explore the environmental controls on the trace metal incorporation
484 at the time of growth. To do this analysis we compare the Mg/Li ratio to parameters that may
485 influence Mg incorporation during precipitation, including salinity, carbonate ion concentration,
486 and temperature.

487 Recent studies have highlighted the potential control of salinity on Mg incorporation in
488 calcitic foraminifera (Kisakurek et al., 2008; Ferguson et al., 2008). Despite a wide salinity range
489 of 34.04 to 36.54 ‰, we do not see any correlation between salinity and Mg/Ca or Mg/Li in our
490 samples (Figure 6). The carbonate ion concentration has also been shown to play a controlling
491 role on Mg/Ca (Martin et al., 2002; Elderfield et al., 2006; Rosenthal et al., 2006) and on Mg/Li
492 in foraminifera (Bryan & Marchitto, 2008). We compare our data to $[\Delta CO_3]$, following the
493 convention of previous discussions (Elderfield et al., 2006; Rosenthal et al., 2006; Bryan &
494 Marchitto, 2008). This value is calculated using derived $[CO_3]$ values from in situ data (Key et
495 al., 200$) and equations from Broecker & Peng (1982), where $[\Delta CO_3] = [CO_3]_{in\ situ} -$
496 $[CO_3]_{saturation}$ and for aragonite, $[CO_3]_{saturation} = 120*e^{(0.16(Z-4))}$ where Z is the depth in km. We
497 find no significant correlation between $[\Delta CO_3]$ and the Mg/Ca, Li/Ca, or Mg/Li ratios (Figure 6).
498 In all cases there is no improvement in correlation whether we differentiate by species or by
499 ocean basin.

500 The correlation between Mg/Li and temperature gives an R^2 value of 0.62 with all 34 data
501 points, and 0.82 when we exclude two visibly chalky coral samples (Figure 7a, b). The only
502 comparable Mg/Li data set comes from Bryan & Marchitto (2008), who measured the Mg/Li

503 ratio of the aragonitic foraminifera, *Hoeglundina elegans*, and found a similar temperature
504 correlation (Bryan & Marchitto, 2008; Figure 7b).
505 There does not appear to be any clear difference between data from solitary
506 (*Desmophyllum*, *Balanophyllia, Caryophyllia, Flabellum,* and *Trochocyanthus*) versus colonial
507 (*Enallopsammia* and *Lophelia*) coral groups (Figure 7a). Our in situ laser ablation data set
508 showed some subtle differences between the geochemistry of *D. dianthus* and *Balanophyllia*, so
509 secondly we consider only *Desmophyllum dianthus* and *Caryophyllia spp.* which are both within
510 the *Caryophyllidae* family and have similar skeletal architecture. Within this subset of corals
511 (n=25, 22 of which are *D. dianthus*) we show an almost identical correlation as when all species
512 are combined (Figure 7a, c). This result is not surprising since 25 of our 34 samples are either *D.*
513 *dianthus* or *Caryophyllia spp*. Again correlations of R^2=0.68 including all 25 and R^2=0.82
514 excluding one chalky sample demonstrate a strong control of temperature on the Mg/Li ratio of
515 these corals. As a third approach, we examine *Caryophyllidae* family corals by ocean basin to
516 see whether sample provenance plays a role in the Mg/Li-to-temperature correlation. There are
517 no obvious differences in the Mg/Li ratio from basin to basin demonstrating that the temperature
518 control is global in nature (Figure 7d). In addition, if we only consider live-collected or
519 radiocarbon dated samples in this analysis the resulting relationship to temperature does not
520 change.
521 We now consider factors that might account for the positive relationship between Mg/Li
522 and temperature. Our laser data show that COC regions have higher Mg/Li than fibrous regions
523 (Figure 4). Increasing the amount of COCs relative to fibrous regions could, therefore, raise the
524 overall coral Mg/Li ratio, essentially linear mixing between two endmembers (Sinclair & Risk,
525 2006). The most extreme measured Mg/Li values in DMC08 are 0.17 mol/mmol and 0.27

526 mol/mmol, but we observe values greater than 0.3 mol/mmol in some corals allowing us to rule
527 out this simple explanation.

528 As an alternative explanation, we examine the combined effect of Rayleigh fractionation
529 and temperature-driven changes to D_{Mg} and D_{Li}. For most of the coral skeleton, Mg/Ca and Li/Ca
530 ratios are consistent with Rayleigh fractionation. Since both Mg and Li are strongly
531 discriminated against during skeletal precipitation, Mg and Li concentrations are predicted to
532 remain nearly constant in the ECF regardless of the extent of precipitation. Thus Mg/Li ratios
533 minimize the effect of Rayleigh fractionation, allowing the expression of other biomineralizing
534 processes and/or environmentally driven changes to Mg/Li

535 If our Rayleigh interpretation is accurate, then the apparent relationship between Mg/Li
536 and temperature could be caused by a temperature dependence of D_{Mg} or D_{Li}. For this
537 mechanism to be consistent with our data, increasing temperature would need to cause an
538 increase in the ratio of D_{Mg} to D_{Li} by changing one or both parameters There are few studies that
539 attempt to quantify D_{Li} or D_{Mg} in inorganic aragonite, and even fewer that explore their
540 temperature dependence. Regarding D_{Mg}, Gaetani & Cohen (2006) report a decrease in D_{Mg} with
541 increasing temperature over the appropriate range for inorganically precipitated aragonite. By
542 contrast, Reynaud et al. (2007) document a 1.6-fold increase of Mg/Ca over 10°C using cultured
543 shallow water corals. Similarly coral aragonite exhibits a D_{Li} decrease of a factor of ~2 over
544 10°C (Marriott et al., 2004a; Marriott et al., 2004b). We are not aware of any data that measured
545 D_{Li} in inorganically precipitated aragonite. For both D_{Mg} and D_{Li} the coral experiments were
546 performed in the range 20-30°C, and there are no empirical data at lower temperatures. Although
547 the data are conflicting there do appear to be temperature dependencies of D_{Mg} and D_{Li} in
548 inorganic and coral aragonite. Thus we can conclude that a temperature dependence of the ratio

549 D_{Mg}/D_{Li} may cause our observed Mg/Li to temperature correlation but we cannot ascertain the
550 controlling mechanism on these distribution coefficients.
551
552 *4.4 Mg/Li as a potential temperature proxy*
553
554 Empirical Mg/Li-to-temperature relationships for deep-sea corals suggest a control by
555 temperature. This ratio is readily measureable by laboratories with trace metal analytical
556 capabilities and can be analyzed on ~10 mg subsamples with a reasonable reproducibility
557 although larger-featured samples may be preferable on large corals. As such it is an appealing
558 candidate for a new paleothermometer in aragonitic deep-sea corals. The equation of the best fit
559 line of the *Caryophyllidae* family corals (*D. dianthus* and *Caryophyllia spp*) (Figure 8c) is:
560
561 $$\text{Mg/Li (mol/mmol)} = 0.009\pm0.0008\text{T (°C)} + 0.19\pm0.006 \quad (4)$$
562
563 On average (excluding the one *Caryophyllidae* chalky sample), the corals exhibit 0.012
564 mol/mmol scatter from the Mg/Li trendline, equivalent to ±1.3°C. When the one *Caryophyllidae*
565 chalky sample is included this scatter increases to 0.014 mol/mmol or ±1.6°C. Some of this
566 range may be due to uncertainty in the ambient seawater temperature that was taken from global
567 data sets and not from the exact location of the coral.
568
569 **5. Conclusion**
570
571 Our results demonstrate that the microscale distributions of Mg/Ca and Li/Ca vary
572 similarly in two genera of deep-sea scleractinian corals. The Mg/Li ratio therefore exhibits lower

amplitude variation. Our data are consistent with trace metal incorporation that varies according to Rayleigh fractionation with a potential role for trace metal association with ACC or organic matter depending upon skeletal architecture.

Solution ICP-MS analyses from ~10 mg samples of 34 corals show less variability in the Mg/Li ratio than Mg/Ca. Neither salinity nor carbonate ion concentration seem to control the Mg/Li ratio. However, temperature correlates to Mg/Li with R^2=0.62 for all corals and with R^2=0.82 for the *Caryophyllidae* family alone. We therefore suggest a temperature control on Mg/Li, but note that paleotemperatures cannot be reconstructed to better than ±1.6°C if using the *Caryophyllidae* trendline.

Acknowledgements

We would like to acknowledge Nicholas White, Rhian Waller and Stephen Cairns (Smithsonian Museum of Natural History) for supplying samples used in this study. In addition Nithya Thiagarajan and Eleni Anagnostou for help in sample selection. Scot Birdwhistell provided support for the ICP-MS analyses. Two anonymous reviewers provided insightful comments that helped to improve the manuscript. Financial Support was provided by the USGS-WHOI Co-operative agreement, NSF-ANT grant numbers 0636787 and 80295700 and the WHOI Ocean Life Institute. David Case was supported by the WHOI Summer Student Fellowship.

References

596 Addadi, L., Raz, S., Weiner, S., 2003. Taking Advantage of Disorder: Amorphous Calcium
597 Carbonate and Its Roles in Biomineralization. Advanced Materials 15, 959-970.
598 Adkins, J.F., Boyle, E.A., Curry, W.B., Lutringer, A., 2003. Stable isotopes in deep-sea corals
599 and a new mechanism for "vital effects". Geochimica et Cosmochimica Acta 67, 1129-
600 1143.
601 Allison, N., Finch, A.A., Webster, J.M., Clague, D.A., 2007. Palaeoenvironmental records from
602 fossil corals: the effects of submarine diagenesis on temperatureand climate estimates.
603 Geochimica et Cosmochimica Acta 71, 4693-4703.
604 Amiel, A.J., Friedman, G.M., Miller, D.S., 1973. Distribution and nature of incorporation of
605 trace elements in modern aragonitic corals. Sedimentology 20, 47-64.
606 Bice, K., Layne, G., Dahl, K. 2005. Application of secondary ion mass spectrometry to the
607 determination of Mg/Ca in rare, delicate, or altered planktonic foraminifera: examples
608 fromt eh Holocene, Paleogene, and Cretaceous. Geochemistry, Geophysics, Geosystems
609 6, Q12PO7.
610 Boyle, E., 1983. Manganese carbonate overgrowths on foraminifera tests. Geochimica et
611 Cosmochimica Acta 47, 1815-1819.
612 Brahmi, C., Meibom, A., Smith, D.C., Stolarski, J., Auzoux-Bordenave, S., Nouet, J., Doumenc,
613 D., Djediat, C., and Domart-Coulon, I. 2010. Skeletal growth, ultrastructure and
614 composition of the azooxanthellate scleractinian coral *Balanophyllia regia*. Coral Reefs
615 29, 175-189.
616 Broecker, W.S., Peng, T.H., 1982. Tracers in the sea. Eldigio (Lamont-Doherty).
617 Bryan, S.P., Marchitto, T.M., 2008. Mg/Ca-temperature proxy in benthic foraminifera: New
618 calibrations from the Florida Straits and a hypothesis regarding Mg/Li. Paleoceanography
619 23, PA2220.
620 Burke, A., Robinson, L. F., Gerlach, D. S., Jenkins, W. J., McNichol, A. P., and Scanlon, K. M.,
621 in press, available online. Reconnaissance dating: A new radiocarbon method applied to
622 assessing the temporal distribution of Southern Ocean deep-sea corals. Deep Sea
623 Research.
624 Cairns, S.D., 2007. Deep-water corals: An overview with special reference to diversity and
625 distribution of deep-water scleractinian corals. Bulletin of Marine Sciences 81, 311-322.
626 Cheng, H., Adkins, J., Edwards, R.L., Boyle, E.A., 2000. U-Th dating of deep-sea corals.
627 Geochimica et Cosmochimica Acta 64, 2401-2416.
628 Cohen, AL., Gaetani, G.A., Lundalv, T., Corliss, B.H., George, R.Y., 2006. Compositional
629 variability in a cold-water scleractinian, *Lophelia pertusa*: new insights into "vital
630 effects". Geochemistry, Geophysics, Geosystems 7, Q12004.
631 Cuif, J.P., Dauphin, Y., Doucet, J., Salome, M., Susini, J., 2003. XANES mapping of organic
632 sulfate in three scleractinian coral skeletons. Geochimica et Cosmochimica Acta 67, 75–
633 83.
634 Elderfield, H., Yu, J., Anand, P., Kiefer, T., Nyland, B., 2006. Calibrations for benthic
635 foraminiferal Mg/Ca paleothermometry and the carbonate ion hypothesis. Earth and
636 Planetary Science Letters 250, 633-649.
637 Erez, J., and Braun, A., 2007. Calcification in hermatypic corals is based on direct seawater
638 supply to the biomineralization site. Geochimica et Cosmochimica Acta 71, A260.
639 Fallon, S.J., McCulloch, M.T., Alibert, C., 2003. Examining water temperature proxies in Porites
640 corals from the Great Barrier Reef: A cross-shelf comparison. Coral Reefs 22, 389-404.

641 Ferguson, J.E., Henderson, G.M., Kucera, M., Rickaby, R.E.M., 2008. Systematic change of
642 foraminiferal Mg/Ca ratios across a strong salinity gradient. Earth and Planetary Science
643 Letters 265, 153-166.
644 Finch, A.A., Allison, N., 2008. Mg structural state in coral aragonite and implications for the
645 paleoenvironmental proxy. Geophysical Research Letters 35, L08704.
646 Gaetani, G.A., Cohen, A.L., 2006. Element partitioning during precipitation of aragonite from
647 seawater: a framework for understanding paleoproxies. Geochimica et Coscmochimica
648 Acta 70, 4617-4634.
649 Gagnon, A.C., Adkins, J.F., Fernandez, D.P., Robinson, L.F., 2007. Sr/Ca and Mg/Ca vital
650 effects correlated with skeletal architecture in a scleractinian deep-sea coral and the role
651 of Rayleigh fractionation. Earth and Planetary Science Letters 261, 280-295.
652 Ganachaud, A., Wunsch, C., 2000. Improved estimates of global ocean circulation, heat transport
653 and mixing from hydrographic data. Nature 408, 453-457.
654 Gladfelter, E.H., 1982. Skeletal development in *Acropora cervicornis*: I. Patterns of calcium
655 carbonate accretion in the axial corallite. Coral Reefs 1, 45-51.
656 Gladfelter, E.H., 2007. Skeletal development in *Acropora palmata* (Lamarck 1816): a scanning
657 electron microscope (SEM) comparison demonstrating similar mechanisms of skeletal
658 extension in axial versus encrusting growth. Coral Reefs 26, 883-892.
659 Grootes, P.M., Stuiver, M., White, J.W.C., Johnsen, S., Jouzel, J., 1993. Comparison of oxygen
660 isotope records from the GISP2 and GRIP Greenland ice cores, Nature 366, 552-554.
661 Johnson, K.S., 1982. Carbon dioxide hydration and dehydration kinetics in seawater. Limnology
662 and Oceanography 27, 849-855.
663 Key, R.M., Kozyr, A., Sabine, C.L., Lee, K., Wanninkhof, R., Bullister, J.L., Feely, R.A.,
664 Millero, F.J., Mordy, C., Peng, T.H., 2004. A global ocean carbon climatology: Results
665 from Global Data Analysis Project (GLODAP). Global Biogeochemical Cycles 18.
666 Kisakürek, B., Eisenhauer, A., Böhm, F., Garbe-Schönberg, D., and Erez, J., 2008. Controls on
667 shell Mg/Ca and Sr/Ca in cultured planktonic foraminiferan, *Globigerinoides ruber*
668 (white). Earth and Planetary Science Letters 273, 260-269.
669 Lea, D., Pak, D., Paradis, G., 2005. Influence of volcanic shards on foraminiferal Mg/Ca in a
670 core from the Galapagos region. Geochemistry, Geophysics, Geosystems 6, Q11P04.
671 Marriott, C.S., Henderson, G.M., Belshaw, N.S., and Tudhope, A.W., 2004a. Temperature
672 dependence of δ^7Li, δ^{44}Ca and Li/Ca during growth of calcium carbonate. Earth and
673 Planetary Science Letters 222, 615-624.
674 Marriott, C.S., Henderson, G.M., Crompton, R., Staubwasser, M., Shaw, S., 2004b. Effect of
675 mineralogy, salinity, and temperature on Li/Ca and Li isotope composition of calcium
676 carbonate. Chemical Geology 212, 5-15.
677 Martin, P.A., Lea, D.W., Rosenthal, Y., Shackleton, N.J., Sarnthein, M., Papenfuss, T., 2002.
678 Quaternary deep sea temperature histrionics derived from benthic foraminiferal Mg/Ca.
679 Earth and Planetary Science Letters 198, 193-209.
680 McConnaughey, T., 1989. ^{13}C and ^{18}O isotopic disequilibrium in biological carbonates: II. *In*
681 *vitro* simulation of kinetic isotope effects. Geochimica et Cosmochimica Acta 53, 163-
682 171.
683 McCulloch, M., Fallon, S., Wyndham, T. Hendy, E., Lough, J., Barnes, D., 2003. Coral record of
684 increased sediment flux to the inner Great Barrier Reef since European settlement. Nature
685 421, 727-730.

686 Meibom, A., Cuif, J-P., Hillion, F., Constantz, B.R., Julliet-Leclerc, A., Dauphin, Y., Watanabe,
687 T., Dunbar, R.B., 2004. Distribution of magnesium in coral skeleton. Geophysical
688 Research Letters 31, L23306.
689 Mitsuguchi, T., Matsumoto, E., Abe, O., Uchida, T., Isdale, P., 1996. Mg/Ca thermometry in
690 coral skeletons. Science 274, 961-963.
691 Mitsuguchi, T., Dang, P.X., Kitagawa, H., Uchida, T., Shibata, Y., 2008. Coral Sr/Ca and Mg/Ca
692 records in Con Dao Island off the Mekong Delta: Assessment of their potential for
693 monitoring ENSO and East Asian monsoon. Global and Planetary Change 63, 341-352.
694 Okumura, M., Kitano, Y., 1986. Coprecipitation of alkali metal ions with calcium carbonate.
695 Geochimica et Cosmochimica Acta 50, 49-58.
696 Politi, Y., Batchelor, D.R., Zaslansky, P., Chmelka, B.F., Weaver, J.C., Sagi, I., Weiner, S.,
697 Addadi, L., 2010. Role of Magnesium Ion in the Stabilization of Biogenic Amorphous
698 Calcium Carbonate: A Structure-Function Investigation. Chemistry of Materials 22, 161-
699 166.
700 Puverel, S., Tambutte, E., Pererra-Mouries, L., Zoccola, D., Allemand, D., Tambutte, S., 2005.
701 Soluble organic matrix of two Scleracti- nian corals: partial and comparative analysis.
702 Comp. Biochem. Physiol., Part B Biochem. Mol. Biol. 141, 480–487.
703 Quinn, T.M., Sampson, D.E., 2002. A multiproxy approach to reconstructing sea surface
704 conditions using coral skeleton geochemistry. Paleoceanography 17, 1062.
705 Rahmstorf, S., 2002. Ocean circulation and climate during the past 120,000 years. Nature 419,
706 207-214.
707 Robinson, LF., Adkins, J.F., Fernandez, D.P., Burnett, D.S., Wang, S.L., Gagnon, A., Krakauer,
708 N., 2006. Primary U distribution in scleractinian corals and its implications for U series
709 dating. Geochemistry Geophysics Geosystems 7, Q05022.
710 Rollion-Bard, C., Vigier, N., Meibom, A., Blamart, D., Reynaud, S., Rodolfo-Metalpa, R.,
711 Martin, S., Gattuso, J., 2009. Effect of environmental conditions and skeletal
712 ultrastructure on the Li isotopic composition of scleractinian corals. Earth and Planetary
713 Science Letters 286, 63-70.
714 Rollion-Bard, C., Blamart, D., Cuif, J-P., Dauphin, Y., 2010. *In situ* measurements of oxygen
715 isotopic composition in deep-sea coral, *Lophelia pertusa*: Re-examination of the current
716 geochemical models of biomineralization. Geochimica et Cosmochimica Acta 74, 1338-
717 1349.
718 Rosenthal, Y., Lear, C.H., Oppo, D.W., Linsley, B.K., 2006. Temperature and carbonate ion
719 effects on Mg/Ca and Sr/Ca ratios in benthic foraminifera: The aragonitic species
720 *Hoeglundina elegans*. Paleoceanography 21, PA1007.
721 Sinclair, D.J., Williams, B., Risk, M., 2006. A biological origin for climate signals in corals -
722 Trace element "vital effects" are ubiquitous in Scleractinian coral skeletons. Geophysical
723 Research Letters 33.
724 Sinclair, D.J., and Risk, M.J., 2006. A numerical model of trace-element coprecipitation in a
725 physicochemical calcification system: Application to coral biomineralization and trace-
726 element ‘vital effects’. Geochimica et Cosmochimica Acta 70, 3855-3868.
727 Smith, J.E., Schwarcz, H.P., Risk, M.J., McConnaughey, T.A., Keller, N., 2000.
728 Paleotemperatures from deep-sea corals. Palaios 15, 25-32.
729 Smith, J.E., Schwarcz, H.P., Risk, M.J., 2002. Patterns of isotopic disequilibria in
730 azooxanthellate coral skeletons. Hydrobiologia 471, 111-115.

731 Steinke, S., Groeneveld, J., Johnstone, H., Rendle-Bühring, R., 2010. East Asian summer
732 monsoon weakening after 7.5 Ma: Evidence from combined planktonic foraminifera
733 Mg/Ca and $\delta^{18}O$ (ODP Site 1146; northern South China Sea). Palaeogeography,
734 Palaeoclimatology, Palaeoecology 289, 33-43.
735 Stoffynegli, P., Mackenzie, F.T., 1984. Mass balance of dissolved lithium in the oceans.
736 Geochimica et Cosmochimica Acta 48, 859-872.
737 Stolarski, J., 2003. Three−dimensional micro− and nanostructural characteristics of the
738 scleractinian coral skeleton: A biocalcification proxy. Acta Palaeonoto Logica Polonica
739 48, 497-530.
740 Walls, R.A., Ragland, P.C., Crisp, E.L., 1977. Experimental and natural early diagenetic
741 mobility of Sr and Mg in biogenic carbonates. Geochimica et Cosmochimica Acta 41,
742 1731-1737.
743 Wang, D., Wallace, A.F., De Yoreo, J.J., Dove, P.M., 2009. Carboxylated molecules regulate
744 magnesium content of amorphous calcium carbonates during calcification. Proceedings
745 of the National Academy of Sciences 106, 21511-21516.

Table 1. All samples analyzed including their identifying information, biology, environmental parameters, and measured trace metal content. The completely averaged bulk solution Me/Me ratios are reported for every coral. Where more than one subsample was analyzed, the average values for each subsample are also presented. Collection temperature is assumed to be growth temperature since corals were either collected live or dated to be modern. Uncertainty in temperature is given in the table. Uncertainty in Mg/Ca, Li/Ca, and Mg/Li are ±0.5 mmol/mol, ±0.01 mol/mmol, and ±1.2 µmol/mol, respectively, based on the maximum likely error (Figure 5).

Lab Label	Cruise Label	Genera	Species	Depth (m)	Latitude (°)	Longitude (°)	Salinity (‰)	$[\Delta CO_3]$ (µmol/kg)	Temperature (°C)	ΔT(°C)	Mg/Ca (mmol/mol)	Li/Ca (µmol/mol)	Mg/Li (mol/mmol)
DMC01	NBP0805-DR34-Dc-A-002	*Desmophyllum*	*dianthus*	869	-59.4	-60.4	34.36	-28.11	1.75	0.05	2.19	10.50	0.209
	a										1.78	8.33	0.213
	b										2.60	12.67	0.205
DMC05	NBP0805-DR35-Dc-A-001	*Desmophyllum*	*dianthus*	695	-59.4	-68.5	34.27	12.60	2.30	0.16	2.90	14.01	0.207
	a										2.76	13.40	0.206
	b										3.04	14.61	0.208
DMC08	NBP0805-TB08-BigBeauty-A	*Desmophyllum*	*dianthus*	816	-54.4	-62.1	34.29	-27.33	3.20	0.16	2.17	9.94	0.218
	a										2.05	9.92	0.207
	b										2.34	10.64	0.220
	c										2.17	9.70	0.223
	d										2.13	9.51	0.224
DMC09	NBP0805-DR40-DcA-1	*Desmophyllum*	*dianthus*	1323	-59.4	-68.6	34.65	-4.11	3.15	0.08	2.58	12.61	0.204
DMC10	NBP0805-TB04-DpA-3	*Desmophyllum*	*dianthus*	816	-54.4	-62.1	34.29	-27.33	2.05	0.16	2.67	12.51	0.214
DMC11	NBP0805-TB04-DpA-2	*Desmophyllum*	*dianthus*	816	-54.4	-62.1	34.29	-27.33	3.15	0.16	3.05	12.32	0.247
48738		*Desmophyllum*	*dianthus*	800	37.5	-25.5	35.50	51.80	10.25	0.85	2.31	11.11	0.206
	a										1.77	9.20	0.192
	b										2.81	13.13	0.214
	c										1.98	9.65	0.205
	d										2.66	12.45	0.213
47409		*Desmophyllum*	*dianthus*	659	-54.3	39.2	34.60		1.90	0.01	1.97	9.36	0.211
47413A		*Desmophyllum*	*dianthus*	421	-50.4	167.4	34.93	-36.20	7.30	0.30	3.02	11.36	0.265
80404		*Desmophyllum*	*dianthus*	390	35.3	-4.1	36.15		13.25	0.25	2.31	7.40	0.312
47407D		*Desmophyllum*	*dianthus*	549	-54.5	-129.5	34.29		2.75	0.15	2.63	12.09	0.218
REH_1	H13 DASS03#1	*Desmophyllum*	*dianthus*	1818	37.0	-60.0	34.98	24.75	3.50	0.50	3.06	13.87	0.220
	a										2.99	13.64	0.219
	b										3.13	14.09	0.222
REH_2	H13 DASS03#2	*Desmophyllum*	*dianthus*	1818	37.0	-60.0	34.98	24.75	3.50	0.50	1.81	8.37	0.216
	a										1.83	8.61	0.213
	b										1.79	8.13	0.219
REH_3	H13 DASS03#3	*Desmophyllum*	*dianthus*	1818	37.0	-60.0	34.98	24.75	3.50	0.50	2.58	11.59	0.223
	a										2.45	10.80	0.227
	b										2.70	12.38	0.218
AB132	CE0806 D19A-1a	*Desmophyllum*	*dianthus*	1720	58.0	-21.0	34.89		3.80	0.50	3.51	14.68	0.239
AB133	CE0806 D19A-2	*Desmophyllum*	*dianthus*	1720	58.0	-21.0	34.89		3.80	0.50	3.41	14.99	0.227
80358		*Desmophyllum*	*dianthus*	358	48.0	-8.0	35.53	-56.82	11.10	0.20	3.24	11.59	0.279
48739		*Desmophyllum*	*dianthus*	825	48.0	-7.0	36.54	-31.56	9.60	0.50	2.40	9.51	0.253
19249		*Desmophyllum*	*dianthus*	274	34.0	-120.0	34.04	-35.21	8.10	0.50	2.42	8.31	0.291
83583		*Desmophyllum*	*dianthus*	464	33.0	-128.0	34.11	-24.06	6.00	0.75	1.60	7.05	0.227
84818		*Desmophyllum*	*dianthus*	400	0.0	-90.0	34.72	-13.38	9.76	0.75	2.60	9.09	0.286
94069		*Desmophyllum*	*dianthus*	710	-31.0	-179.0	34.41	-69.47	7.40	0.50	2.61	8.59	0.304
DMC07	NBP0805-TB04-Dry Samples Modern Balan #1	*Balanophyllia*	*malouensis*	816	-54.4	-62.1	34.29	-27.33	3.15	0.16	1.91	9.13	0.209
	a										1.80	8.64	0.208
	b										2.03	9.61	0.211
DMC02	AB011-LMG0605 #20	*Balanophyllia*	*malouensis*	854	-53.5	-59.4	34.30		3.05	0.10	1.96	9.20	0.213
DMC03	QD024-LMG0605-Stn3#1	*Balanophyllia*	*malouensis*	120	-53.5	-61.5	34.21	-23.30	4.89	0.60	2.35	11.19	0.210
DMC04	QD030-LMG0605-Stn9-Box2	*Balanophyllia*	*malouensis*	318	-54.3	-62.1	34.19	-25.34	4.31	0.25	2.15	9.62	0.223
1010252		*Caryophyllia*	*ambrosia caribbeana*	785	28.2	-86.3	34.91	15.18	6.60	0.80	2.48	10.66	0.223
49020A		*Caryophyllia*	*berteriana*	201	12.5	-70.4	35.66	58.43	17.00	0.01	2.68	7.62	0.352
45923		*Caryophyllia*	*ambrosia*	1318	7.4	-56.3	35.00	25.47	4.70	0.30	1.85	9.29	0.199
77019		*Enallopsammia*	*profunda*	494	30.2	-79.6	36.32	124.10	15.50	0.50	2.74	10.84	0.253
47531		*Enallopsammia*	*rostrata*	333	-51.0	162.1	35.00	-35.74	7.30	0.70	3.08	11.95	0.258
DMC06	NBP0805-TB04-Dry Samples Flabellum	*Flabellum*	*curvatum*	816	-54.4	-62.1	34.29	-27.33	3.15	0.16	1.73	8.78	0.197
	a										1.86	9.33	0.199
	b										1.60	8.22	0.194
61768B		*Trochocyanthus*	*rawsonii*	229	2.0	-47.0	35.37	87.37	10.00	2.00	3.29	10.39	0.317
46238I		*Lophelia*	*prolifera*	440	-25.0	-44.0	35.17	102.62	10.00	2.00	3.21	10.56	0.304

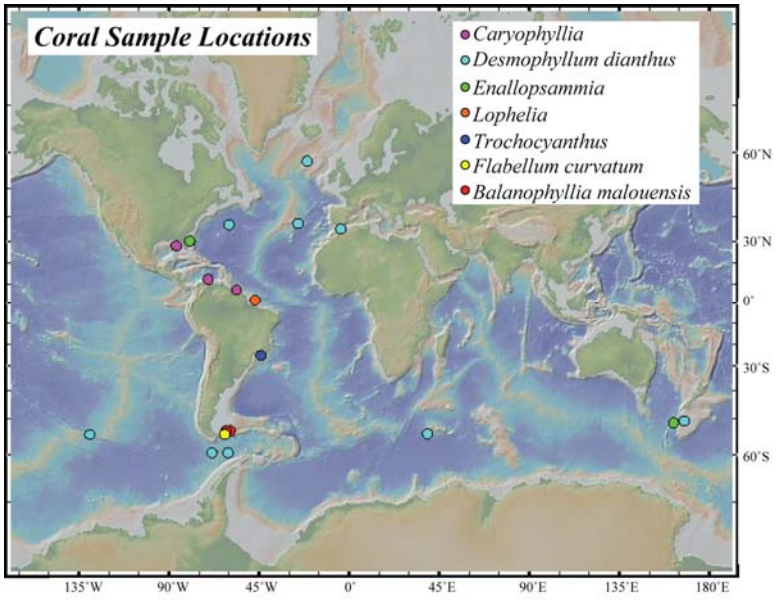

Figure 1. Location of coral sites colored by species. In cases where more than one species came from one site the location was colored according to the majority species found there (Table 1).

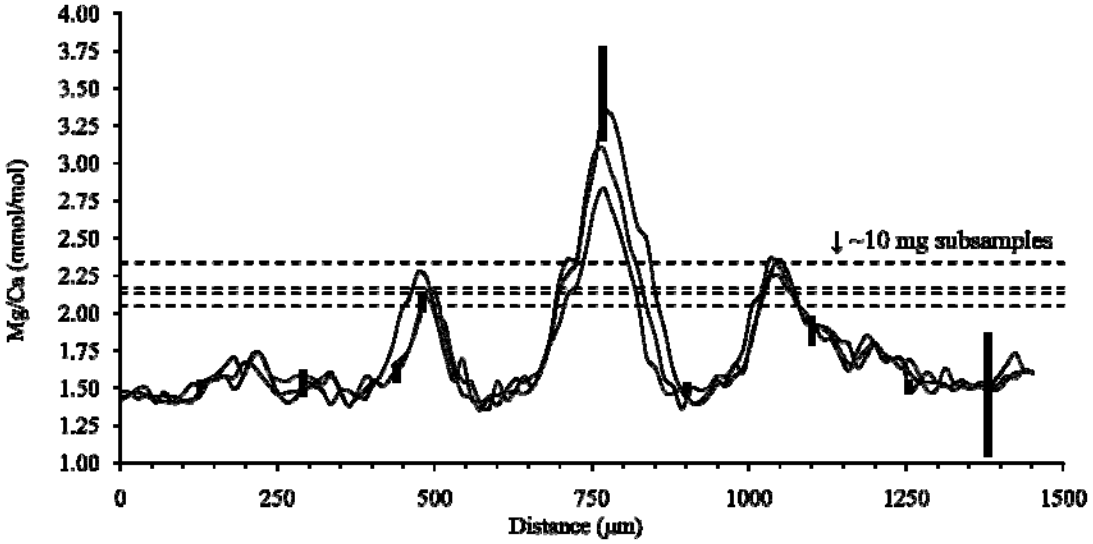

Figure 2. The Mg/Ca ratios analyzed in *D. dianthus* sample DMC08. Thin black lines are the closely spaced "long" laser lines run perpendicular to coral density strata. Thick black vertical bars are the Mg/Ca value from "short" laser lines. The length of the bar represents the uncertainty in those values. The four horizontal, dashed black lines are the Mg/Ca values obtained from four separate ~10 mg subsamples of the same coral analyzed by solution ICP-MS (Table 1).

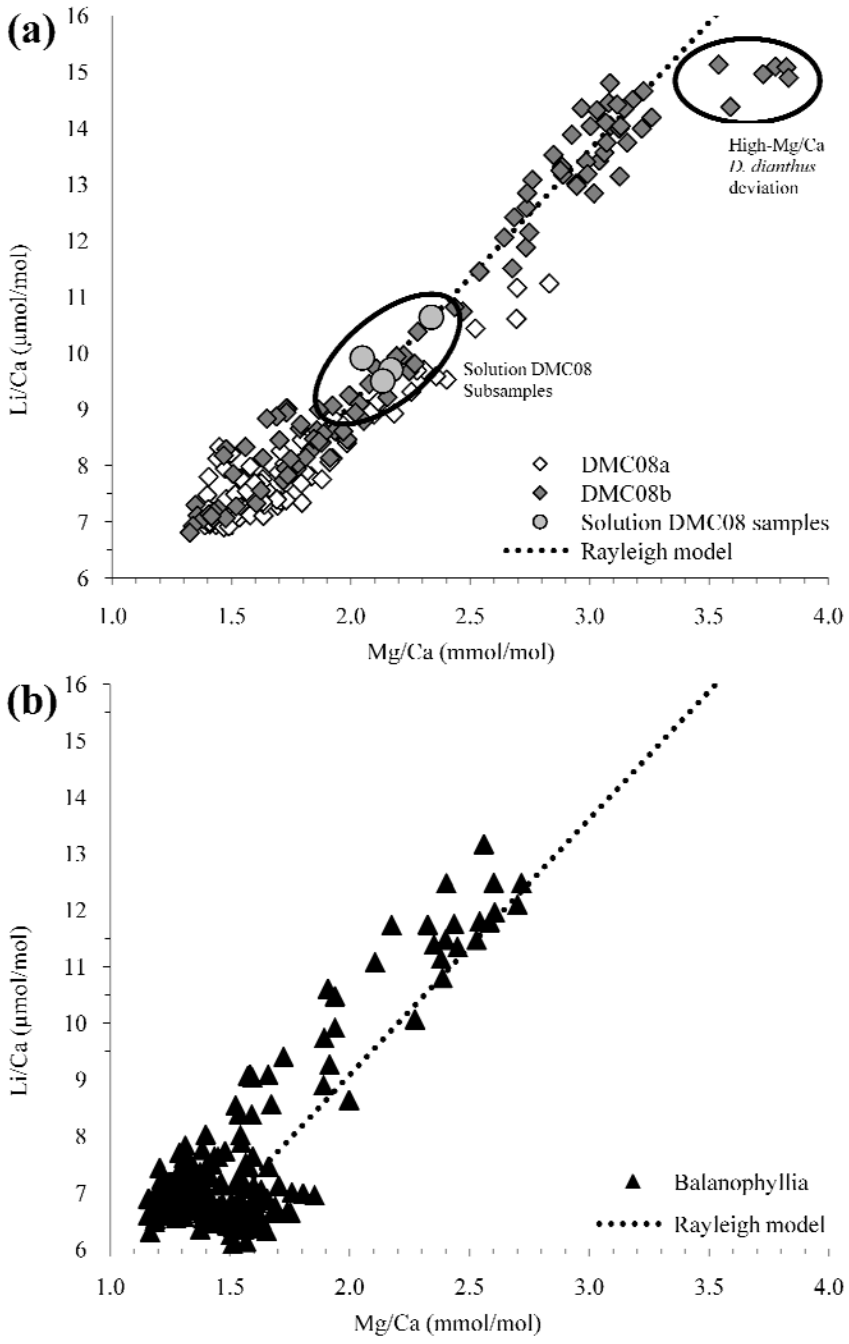

Figure 3. Laser ablation data for **(a)** DMC08a, DMC08b, and **(b)** *Balanophyllia*. Rayleigh models were calculated using D_{Li} of 0.00269 and D_{Mg} of 0.000292. The uncertainty on the solution DMC08 subsamples are smaller than the symbol size, and replicate laser lines have an reproducibility of ~5%.

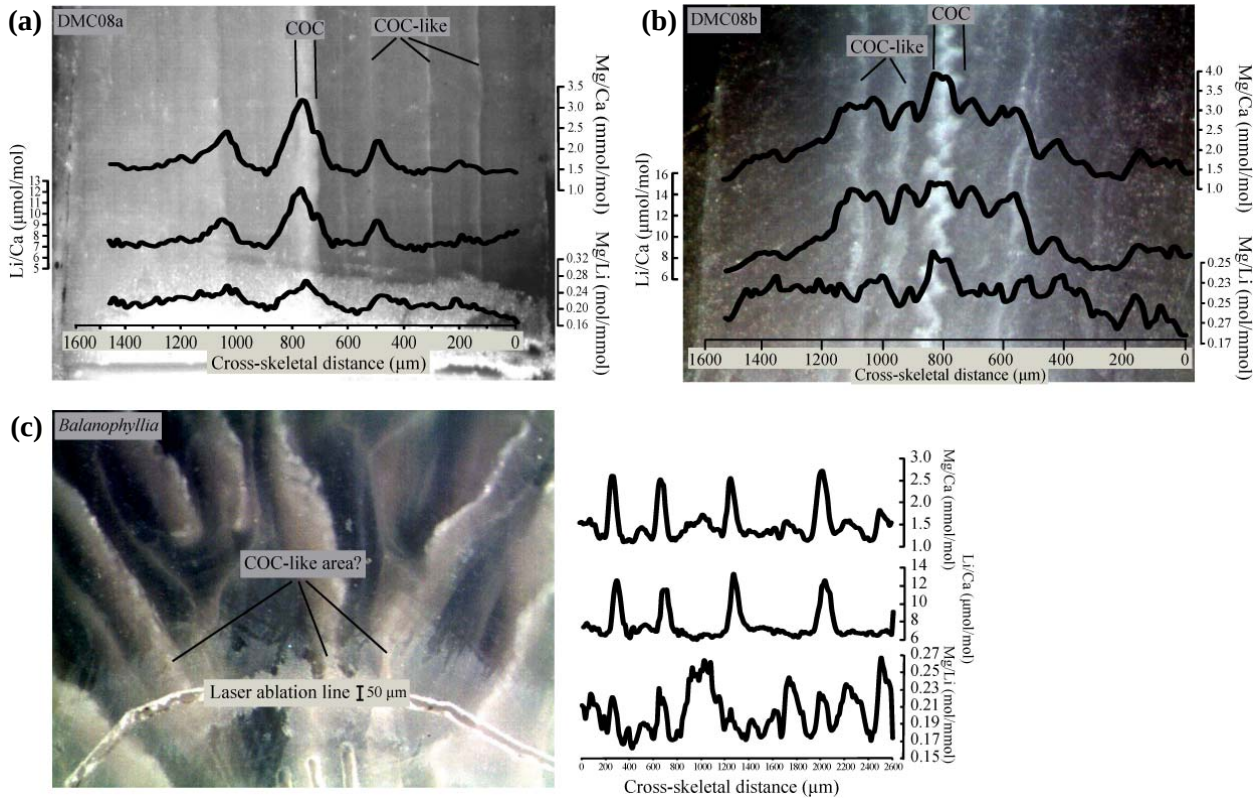

Figure 4. Laser ablation ICP-MS data overlaid on reflected light images of three coral sections. The first two sections **(a)** and **(b)** are from *D. dianthus* DMC08**.** The COCs are well developed and appear white in these sections. The x-axes indicate the location of the laser ablation line. **(c)** *Balanophyllia*. This laser ablation line was curved to stay perpendicular to the complex growth lines. In all cases, adjacent analyses indicate 5% error for Mg/Ca and Li/Ca ratios and 3% for Mg/Li. In addition regions which appear to exhibit similar geochemical behavior to COCs but which are not central to the skeleton are labeled "COC-like."

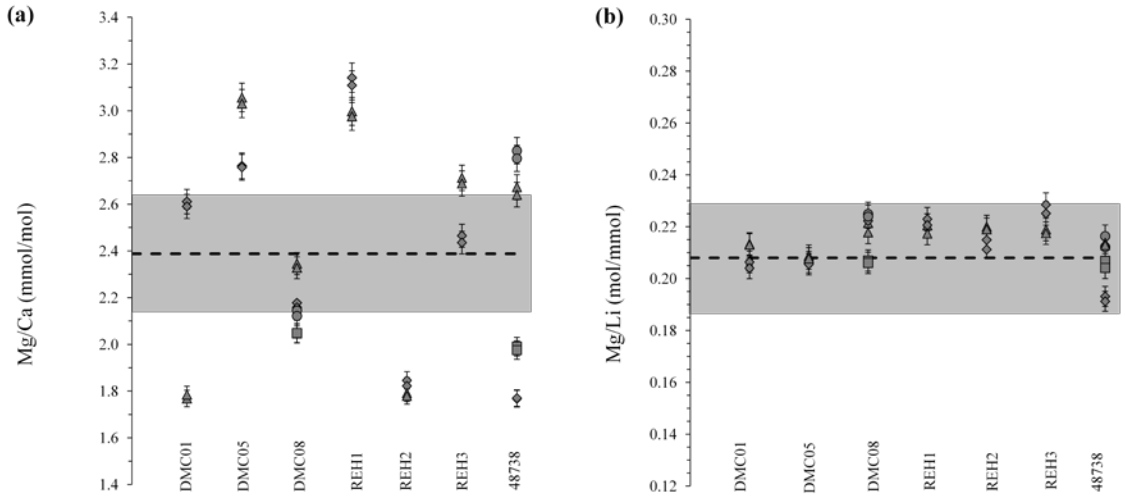

Figure 5. Intra-coral variability. **(a)** Mg/Ca and **(b)** Mg/Li. Only *D. dianthus* replicates are shown here. Within each coral individual symbols differentiate subsamples, while duplicate analyses of the same aliquot have the same symbol. Error bars for Mg/Li and Mg/Ca are 2%, each reflective of the standard deviation of reproducibility standards (S13). The average of plotted values is shown as a dashed line, and the gray box defines 10% deviations above and below the average.

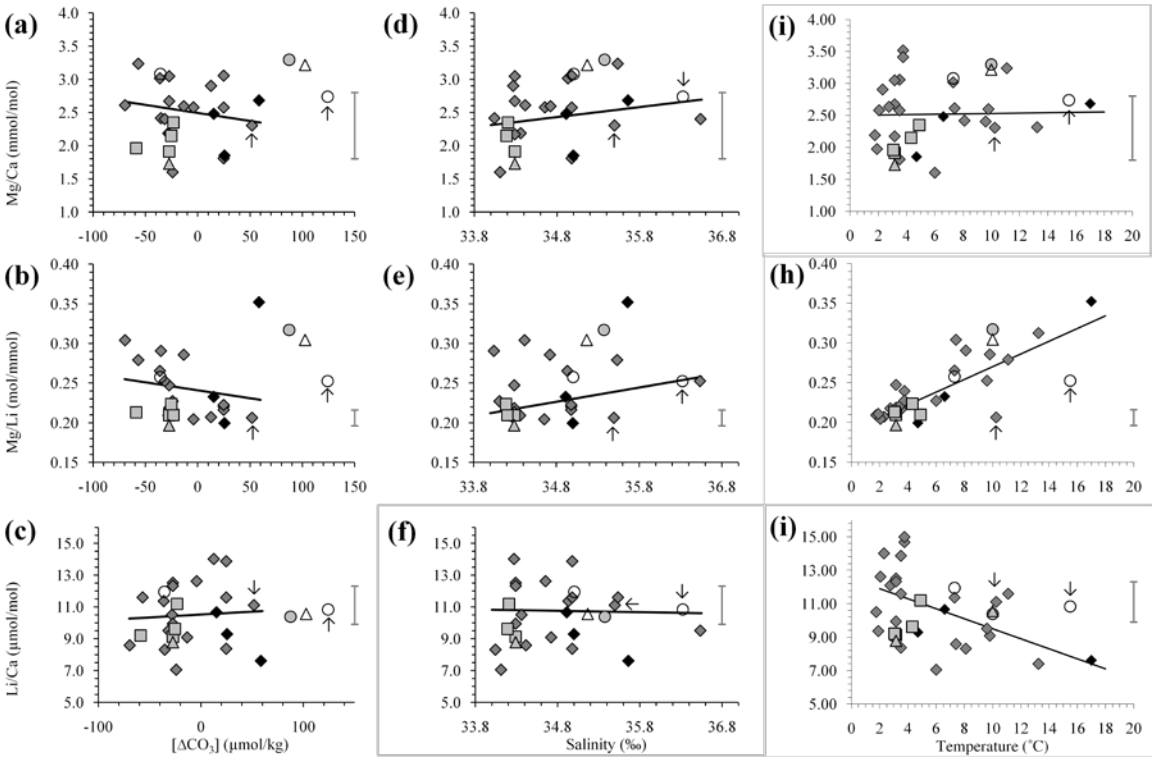

Figure 6. Subplots **(a, b, c)**: effect of carbonate ion concentration on Mg/Ca, Mg/Li, and Li/Ca. Subplots **(d, e, f)**: effect of salinity on the Mg/Ca, Mg/Li, and Li/Ca ratios. Subplots (**g, h, i**): effect of temperature on Mg/Ca, Mg/Li, and Li/Ca. Two chalky samples are shown with arrows. Symbols represent: *D. dianthus* (◆), *Caryophyllia spp.* (◆), *Balanophyllia* (■), *Flabellum* (▲), *Trochocyanthus* (●), *Enallopsammia* (○), *Lophelia* (△). Trendlines are given for the *Caryophyllidae* (◆ + ◆) data, for which the highest [ΔCO_3] value is 58.4. All [ΔCO_3] values are calculated using derived [CO_3] values from in situ GLODAP data and equations from Broecker & Peng (1982). Gray bars at right indicate the maximum likely error in measurement, derived from data shown in Figure 5.

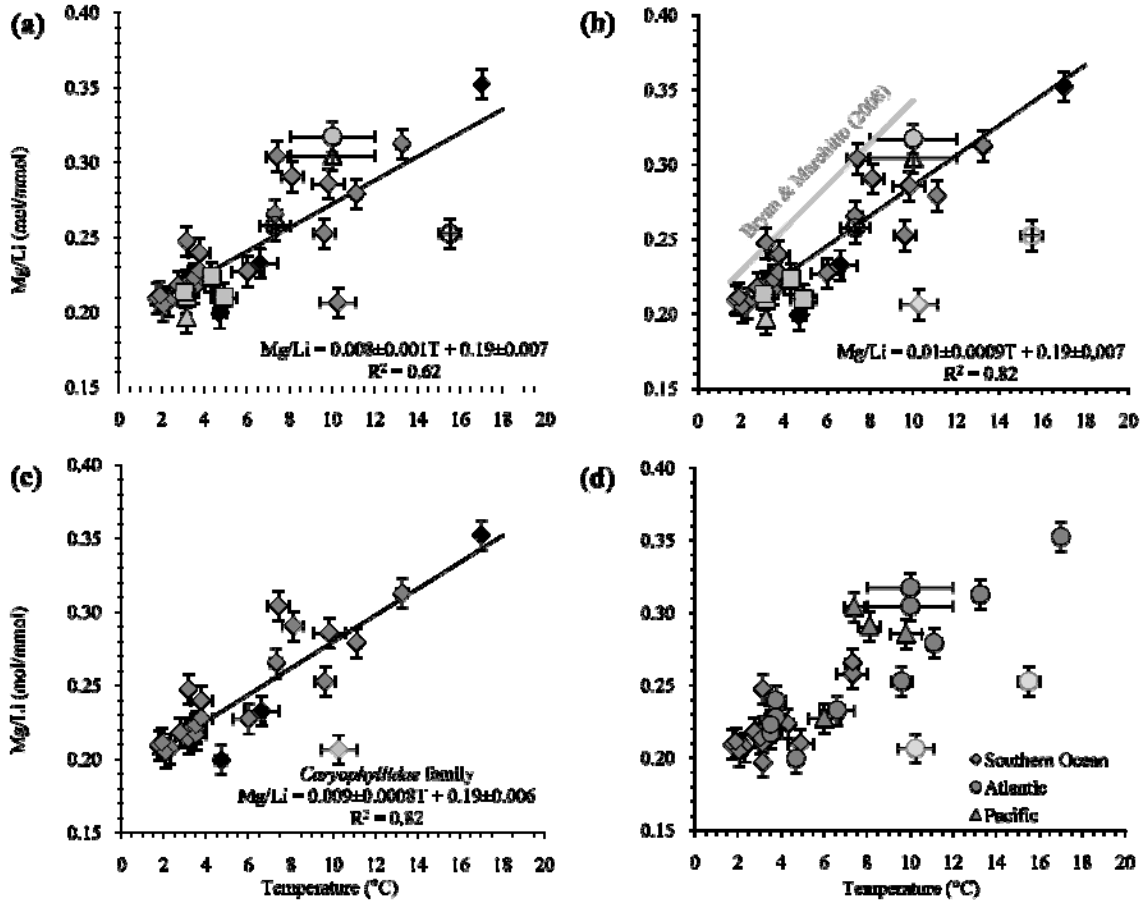

Figure 7. Mg/Li-to-temperature comparisons. Unless indicated in the subplot, symbols represent: *D. dianthus* (◆), *Caryophyllia spp.* (◆), *Balanophyllia* (■), *Flabellum* (▲), *Trochocyanthus* (●), *Enallopsammia* (○), *Lophelia* (△). Subplots display **(a)** Regression given for all data, separated by species; **(b)** Regression with the two visibly chalky samples removed (but shown faintly). The gray line represents the Mg/Li-to-temperature relationship given in Bryan & Marchitto (2008) for the aragonitic foraminifera *H. elegans*; **(c)** Regression for members of the *Caryophyllidae* family with one chalky sample shown faintly and not included in the regression (black line); **(d)** All samples, divided by major ocean basin, two chalky samples shown faintly. Temperature errors are derived from the GLODAP database (Key et al., 2004).